THE JOURNAL OF PHYSICAL CHEMISTRY C

Article

pubs.acs.org/JPCC

Variational Reconstruction of Exciton Multipath Deexcitation Lifetime Spectra in Coupled PbS Colloidal Quantum Dots

Jing Wang[†,‡] and Andreas Mandelis*[,†,‡]

[†]School of Optoelectronic Information, University of Electronic Science and Technology of China, Chengdu, Sichuan 610054, China

[‡]Center for Advanced Diffusion-Wave Technologies (CADIFT), Department of Mechanical and Industrial Engineering, University of Toronto, Toronto M5S 3G8, Canada

ABSTRACT: In typical quantum dot solids used for photovoltaic applications, the dominant source of carrier loss is through trap states. Identifying pathways for exciton relaxation from these states is important to the optimization of energy conversion devices. A generalized variational inverse method for the reconstruction of multipath exciton lifetime spectra in PbS colloidal quantum dots (CQD) used for solar cells was developed which allows for resolving concurrent multipath relaxation lifetime mechanisms in the form of Voigt distributions. The variational inverse method was applied to high signal-to-noise ratio photocarrier radiometric phase frequency responses from coupled CQD assemblies with 0.5−1.0 nm interdot spacings. Two concurrent deexcitation mechanisms with radiative and nonradiative channels were found in the range of 300 K ≥ T ≥ 100 K: Exciton−phonon interaction involving the lowest 1S−1S excitonic state splitting and a thermalization broadening model based on the exciton trapping probability dominated the temperature range of ≥200 K. Exciton hopping in the form of tunneling from a smaller quantum dot in a higher-energy state to a lower-energy state of nearby larger quantum dots dominated temperatures <200 K.

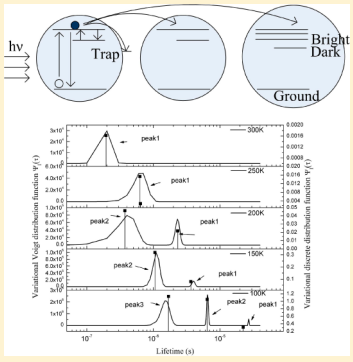

INTRODUCTION

The importance of exciton decay mechanism elucidation of interacting ("coupled") colloidal quantum dots (CQD) is commensurate with their growing use in photonic and optoelectronic device fabrication, such as colloidal solar cells, and can have a substantial impact on the understanding, control, and optimization of the fabrication process. Decoupling these mechanisms has been a major problem in CQD deexcitation physics to date. The size-tunable electronic and optical properties of lead salt (PbS, PbSe, and PbTe) QCDs have made these materials promising candidates for third-generation thin-film photovoltaic systems.[1−3] Studies of the optical-to-electronic energy transfer and subsequent electron transport in lead salt CQDs are critical to understanding and optimizing the fabrication of both thin films and devices.[4] Over the past decade, various exciton deexcitation and transport mechanisms have been discovered. In a coupled QD assembly where the interdot spacing is short, about 0.5−1 nm, Förster resonance energy transfer (FRET)[5] occurs from smaller to larger QDs. Physical processes driving exciton transport range from Coulomb blockade at room temperature to nearest-neighbor hopping (NNH) (near 200 K) and variable-range hopping (VRH) (T < 200 K).[6] Three different temperature regimes over a temperature range of 6−290 K showing different photoluminescence (PL) intensities and decay rates were also found by Andreakou et al.[7] The commonly used dc (or continuous) photoluminescence (PL) lifetime measurements are not suitable for probing dynamic exciton decay processes. Time-resolved PL has been used for the purpose of measuring relaxation lifetimes in PbS QDs at various temperatures.[7−10] However, major problems with this modality persist. They include excessive noise due to the broad bandwidth of fast detectors required to capture the transient, especially at long PL transient times (tens of microseconds), thereby yielding poor lifetime accuracy,[9] and the nonexponential character of the decay which makes use of the deconvolution algorithms' imprecision and resulting poorly resolved lifetimes, only under the unjustified assumption of discrete lifetimes. Reliable physical models of QD excited-state interactions as a function of parameters such as ambient temperature, QD, and trap densities, which are crucial to obtaining a complete physical picture of the details of exciton relaxation mechanisms, have not been possible to date due to the foregoing limitations on lifetime measurement accuracy and precision/resolution.

Significant progress has been made recently through the introduction of photocarrier radiometry (PCR) into PbS CQD thin-film exciton decay dynamics.[11] PCR is a frequency-domain PL modality,[12] the spectral bandwidth of which is gated to eliminate thermal−infrared photon contributions resulting from radiatively emitted photon reabsorption and nonradiative conversion. Moreover, PCR as a nondestructive, noncontacting characterization method can be of considerable importance because the (semi-) soft CQD optoelectronic materials are vulnerable to contacting probe damage during subsequent processing steps. Conventional electrical characterization methods for trap state identification are typically highly

Received: June 22, 2014
Revised: July 27, 2014
Published: July 28, 2014

   dx.doi.org/10.1021/jp506194y | J. Phys. Chem. C 2014, 118, 19484−19491

convoluted and require carefully controlled experiments. In contrast, nondestructive optical characterization methods typically probe the bulk of the materials, which can provide information on the nature of the material without side effects. Both PCR and time-resolved PL can yield quantitative information about relaxation lifetime distributions and their radiative and nonradiative components associated with intra-QD and inter-QD excited-state decay processes.[9,11] However, PCR phase data with a maximum variance of 0.43% for a coupled PbS CQD sample suggest that the accuracy and precision of PCR is much superior to that of time-resolved PL which has a typical uncertainty range of 1.7−17%.[9] This is due to the intrinsically high signal-to-noise ratio (SNR) of PCR based on narrow band lock-in demodulation and has to do with the fact that the demodulated phase is the ratio of the two lock-in signals, quadratue (Q) and in-phase (IP); as a ratio, the phase is generally immune to instrumental signal fluctuations to which the amplitude is sensitive, but they are canceled out of the numerator and denominator of the phase channel. This adds a strong stability advantage to the phase channel. Wang et al.[11] presented a variational formalism for the exciton relaxation time distribution reconstruction inverse problem from the PCR modulation frequency response, leading to two simultaneous integral equations in the lifetime distribution function (spectrum) for the IP and Q lock-in signal channels which were subsequently used to reconstruct the lifetime spectrum. It was shown that highly reproducible discrete lifetime distribution spectra can be obtained for both uncoupled (non-interacting) and coupled thin-film CQD samples. A major problem with discrete lifetime distributions (primitive line spectra) is that they do not yield physical deexcitation mechanisms of interacting excitons nor are they able to differentiate between concurrent relaxation lifetime processes because they result in spectra with multiple independent lifetimes which vary arbitrarily with temperature and which are thus difficult or impossible to analyze in terms of coherent physical processes.

The introduction of a continuous variational lifetime theory into the PCR frequency scans[11] allowed for Voigt lifetime broadening analysis in uncoupled samples, consistent with random size distributions known to exist in colloidal QD films.[13] Unfortunately, this method cannot be applied to the coupled PbS CQD sample which is not amenable to single-peak Voigt distribution analysis. The inability to find an acceptable Voigt fit for the coupled sample at any temperature is hypothesized to be indicative of the multiple deexcitation channel mechanisms associated with simultaneous and possibly interdependent energy decay pathways. Unlike the essentially self-confined uncoupled case, additional relaxation degrees of freedom in the coupled lifetime distribution profiles are likely to involve nearest-neighbor inter-QD interactions in the form of excited-state electron tunneling (nearest-neighbor hopping (NNH) migration or a Föster resonance) resulting in photon emission from another QD. The difficulty arises for the coupled sample due to the expected, more complicated intersystem crossing network leading to a composite lifetime spectrum consisting of more than one relaxation mechanism.

The schematic diagram of the PCR experimental setup is shown in Figure 1. A 10 mW diode laser of 830 nm wavelength and a beam diameter of ca. 0.1 mm was square-wave modulated with a function generator. A 1 μm long-pass filter was placed in front of the InGaAs photodetector to block the excitation beam. No short-pass filter was necessary as thermal infrared

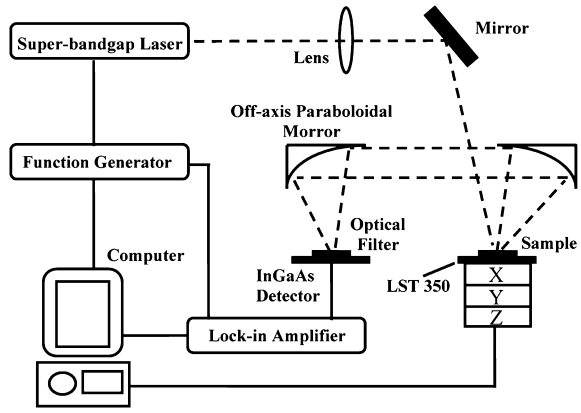

Figure 1. Schematic diagram of the photocarrier radiometry (PCR) setup for CQD frequency and temperature scans (reproduced with permission from ref 11).

contributions to the signal were found to be negligible. The sample was placed on a Linkam LTS350 cryogenic stage, which allows us to maintain constant temperature in the 77−520 K range. Since high temperatures would dramatically and irreversibly change the properties of the PbS CQDs, the highest temperature for frequency and temperature scans was set to 300 K. For a coupled PbS QD thin film with an average diameter of 4.2 nm, fabricated through a layer-by-layer process in which the long oleic acid ligands were displaced by shorter 3-mercaptopropionic acid ligands resulting in an interparticle spacing of ca. 0.5−1 nm,[14] the PCR signals were analyzed in terms of the variationally inverted primitive line spectra and were found to be dominated by radiative emission channels.[11] Nevertheless, the lack of a mathematical methodology to introduce multipath deexcitation lifetime distributions other than the primitive line spectra into the variational method has precluded any distributed and/or simultaneous parallel lifetime spectra reconstruction from the PCR frequency response and the emergence of a physical picture in connection with the mechanisms dominating the spectrum.

VARIATIONAL THEORY OF COUPLED COLLOIDAL QUANTUM DOT EXCITONIC LIFETIME SPECTRA

In this report we develop a generalization of the variational method introduced by Wang et al.[11] for exciton lifetime reconstruction which can handle simultaneous multipath deexcitation mechanisms, thereby allowing for unambiguous physical modeling and the interpretation of the resulting lifetime distributions using the temperature dependencies of the peaks and fwhm of the associated Voigt distributions in coupled CQDs. As there is no diffusive transport across the medium of localized quantum dots, the theory for PCR analysis resulting in eqs 1 and 2 below was based on rate equations and was not developed in the diffusive limit. The method involves a two-stage approach to lifetime calculation: First, a discrete lifetime line spectrum best-fitted to the PCR quadrature (Q-channel) frequency response data is generated from the aforementioned variational formalism to identify approximate values and relative strengths of the dominant lifetime peaks on the relaxation time axis. The reason for considering only the Q channel of the PCR frequency response is that that phase is known to be more sensitive than amplitude to the values of relaxation lifetimes associated with luminescent (radiative) emission processes in optoelectronic systems.[15,16] In addition

dx.doi.org/10.1021/jp506194y | J. Phys. Chem. C 2014, 118, 19484−19491

to the aforementioned phase channel stability, the phase lag is self-normalized and absolute (= 0° at low frequencies) and changes linearly over several decades of frequency, whereas amplitude absolute values are arbitrary (and therefore not very useful; only relative amplitude values are meaningful) and decrease over several orders of magnitude with increasing frequency, thereby suffering from reduced sensitivity to short-lifetime values which require high frequencies to be measured. Therefore, the following discussion is mainly based on best-fitted phase (or, equivalently, quadrature) results. Phase (and quadrature) further provides a self-referenced baseline value of zero at low modulation frequencies, f, where $\omega\tau \ll 1$, with $\omega = 2\pi f$. The PCR Q channel of n frequency-scan data points, $F_I(\omega_i)$, is inverted through[11]

$$\sum_{m=1}^{n} \frac{\beta_m \omega_i {\tau_m}^2}{1 + (\omega_i \tau_m)^2} = -F_I(\omega_i) \quad (1 \le m \le n,\ 1 \le i \le n) \tag{1}$$

where β_m represents the variational coefficients associated with the process (m) and τ_m represents the discrete lifetimes resulting from the inversion. The β_m coefficients are optimized to yield a solution to the $n \times n$ matrix represented by eq 1, resulting from the variational extremization of the functional associated with the Fredholm integral equation[11]

$$\int_0^\infty K_I(\omega\tau)\, \Psi_I(\tau)\, d\tau = F_I(\omega) \quad (0 \le \omega < \infty) \tag{2a}$$

where $\Psi_I(\tau)$ is the lifetime distribution function and the imaginary kernel $K_I(\omega\tau)$ is symmetric and given by

$$K_I(\omega\tau) = -\frac{\omega\tau}{1 + (\omega\tau)^2} \tag{2b}$$

Next, the discrete τ_m spectrum is used as a seed input for the inversion of the generalization of eq 1 to yield a multipath Voigt spectrum which assumes arbitrary broadened lifetime distributions of line width $\Delta\tau_m$. The generalized variational matrix element $H_{I,im}$ is found to be

$$\sum_{m=1}^{n} \beta_m H_{I,im}(\tau_m, \omega_i; \Delta\tau_m, \Delta\omega_i) = S_{Ii}(\omega_i, \Delta\omega_i) \quad (1 \le m \le n,\ 1 \le i \le n) \tag{3a}$$

where

$$S_{Ii}(\omega_i, \Delta\omega_i) = \int_0^\infty F_I(\omega) e^{-[(\omega-\omega_i)/\Delta\omega_i]^2} \omega\, d\omega \tag{3b}$$

$\Delta\omega_i$ is the line width of the Fourier transform of the lifetime distribution: $\Delta\omega_i = 2\pi/\Delta\tau_i$. The generalized formalism yields variationally optimized multiple Voigt lifetime distributions (peaks and fwhm) which allow the reconstruction of a full relaxation spectrum including simultaneously operating exciton deexcitation path mechanisms. Finally, the physical origins of the multipath lifetime spectrum are identified using theoretical models for each simultaneous deexcitation mechanism over various temperature ranges.

The variational solution can be written as a superposition of a series of Gaussian probability distributions with peaks at lifetimes τ_i $(1 \le i \le n)$

$$\Psi_I(\tau) = \sum_{i=1}^{n} \beta_i \tau e^{-[(\tau-\tau_i)/\Delta\tau_i]^2} \quad (i = 1, 2, \ldots n) \tag{3c}$$

where τ_i is the most probable lifetime value. The fitting limits of τ_i are set to a small range around the corresponding discrete lifetime values, while the limits of $\Delta\tau_i$ and β_i can be relatively large. The minimum of the best-fit variance was found by gradually narrowing the limits and increasing the sweeping step. Upon best-fitting the PCR frequency quadrature curves, the results were recast into the signal phase channel (Figure 2b)

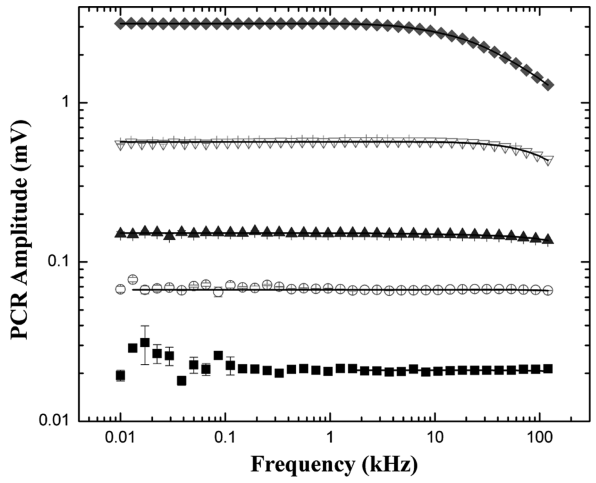

(a)

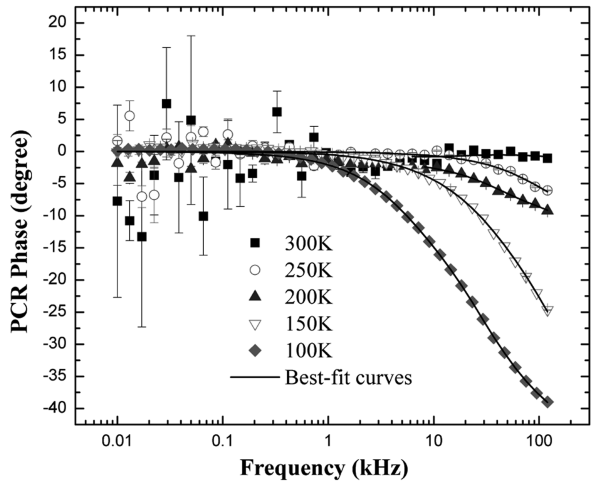

(b)

Figure 2. PCR frequency-scan spectra of the coupled samples at various temperatures. Best-fit curves were calculated from eq 3a. (a) Amplitudes for the coupled sample. (b) Phases for the coupled sample. Error bars, when not apparent, are the same size as, or smaller than, the symbols (reproduced with permission from ref 11).

using eq 3a. The reconstructed spectrum of multiple Voigt exciton lifetime distributions is shown in Figure 3, where the maximum value of the distribution function of each peak can be expressed as $\Psi_{Ii}(\tau)$, $1 \le i \le 3$, as only three dominating lifetime values were found in the discrete spectrum at 100 K. Good agreement was observed between the peaks of the Voigt broadened lifetime distributions and the discrete line spectra, Figure 3, with respect to time localization, which further demonstrates the reliability of the variational lifetime spectrum reconstruction approach. The three center (peak) lifetimes τ_i

dx.doi.org/10.1021/jp506194y | J. Phys. Chem. C 2014, 118, 19484−19491

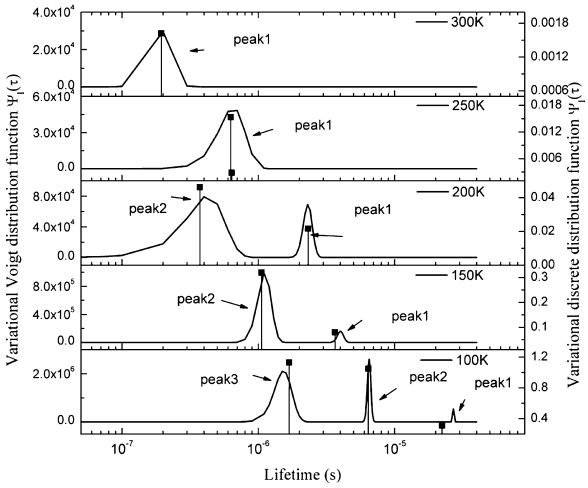

Figure 3. Variational discrete and continuous multiple exciton lifetime distribution spectra of a coupled colloidal PbS quantum dot sample, reconstructed from PCR quadrature-channel frequency-scan data at various temperatures.

and their line widths $\Delta\tau_i$ and the variational solution distribution function $\Psi_I(\tau)$ at five discrete temperatures between 300 and 100 K are shown in Tables 1 and 2, respectively. Using the experimental error bars shown in Figure 2, the maximum and minimum of the standard deviations were also fitted and resulted in the variances shown in Tables 1 and 3. The small error bars show that our PCR method produces stable and precise lock-in signals. The peak magnitude in Figure 3 is interpreted as the relative probability of occurrence of an exciton relaxation event with the given discrete (line) or broadened (Voigt) lifetime distribution. The appearance of a shorter lifetime peak (peak 2) at and below 200 K marks the effective onset of a new deexcitation pathway for PbS CQD excitons which operates simultaneously with the longer decay pathway present at and below 300 K (peak 1). As the temperature decreases, the magnitude of peak 1 diminishes relative to that of peak 2. With further temperature decreases, another shorter lifetime distribution (peak 3) appears at T = 100 K while peak 1 continues to decrease in relative terms. To understand the relative and absolute changes in peak 1 within the framework of multiple simultaneous deexcitation pathway lifetime distributions, the following definitions are made: The relative strength $\eta_1(T)$ of peak 1 at each temperature

$$\eta_1(\mathrm{T}) \equiv \left[\frac{\Psi_{I1}(T)}{\sum_{j=1}^{3}\Psi_{Ij}(T)}\right] \times 100\% \tag{4}$$

and the peak strength ratio $\xi_1(T)$ at temperature T normalized with respect to its value at 300 K:

Table 2. Variational Distribution Function Values for Peak 1 and the Relative Strength and Strength Ratio

T (K)	$\Psi_{I1}(T)$ (a.u.)	η_1 (%)	ξ_1 (%)
300	2.97×10^4	100	100
250	4.84×10^4	100	61.36
200	6.9×10^4	46.56	43.04
150	1.6×10^5	13.91	18.56
100	5.4×10^5	1.14	5.5

$$\xi_1(\mathrm{T}) \equiv \left[\frac{\Psi_{I1}(T = 300\ \mathrm{K})}{\Psi_{I1}(T)}\right] \times 100\% \tag{5}$$

As shown in Table 2, $\Psi_{I1}(T)$ increases with decreasing temperature; however, the relative strength η_1 at each temperature and the peak 1 strength ratio ξ_1 decrease monotonically.

Considering the Voigt distribution results, we find that the decreasing relative strength η_1 with decreasing temperature indicates the emergence of alternative competing exciton decay pathways at T < 200 K which become increasingly important and rate-limiting at lower temperatures. At T = 100 K only 1.14% of all excitons decay radiatively through the mechanism dominating room-temperature decay which is associated with peak 1. Simultaneously, normalized ratio ξ which physically represents the fraction of exciton population decaying through the pathway associated with peak 1 at room temperature to the same pathway at lower temperatures rapidly decreases as a result of overall enhanced low-temperature radiative decays and reaches 5.5% at T = 100 K. The above η_1 and ξ_1 calculations indicate that the dominant room-temperature exciton radiative emission probability is almost 20 times lower than its value at 100 K yet it is only 1.14% of all available radiative deexcitation pathways at that temperature.

To elucidate the physical processes of exciton decay in the presence of multiple competing radiative and nonradiative pathways, we analyze the temperature dependencies of the lifetime distributions, peaks 1 and 2 (Figure 3), as simultaneous exciton decay mechanisms.

RECONSTRUCTION OF THE EXCITONIC MULTIPATH LIFETIME SPECTRUM

Peak 1: Exciton–Phonon Interaction and Thermalization. Wang et al.[11] showed that the single Voigt broadened lifetime distribution in uncoupled PbS CQDs is due to phonon-mediated exciton relaxation dynamics. The PCR technique can resolve both radiative and nonradiative decays through the temperature dependence of the lifetime. A rate equation model involving radiative (R) and nonradiative (NR) decay channels was introduced, and the lifetime expressions are reproduced here

Table 1. Voigt Peak Lifetimes and fwhm at Various Temperatures

T (K)	τ_1 (μs)	$\Delta\tau_1$ (μs)	τ_2 (μs)	$\Delta\tau_2$ (μs)	τ_3 (μs)	$\Delta\tau_3$ (μs)
300	0.18 ± 0.01	0.110 ± 0.015				
250	0.62 ± 0.03	0.210 ± 0.005				
200	2.3 ± 0.05	0.250 ± 0.003	0.380 ± 0.005	0.190 ± 0.003		
150	4.0 ± 0.1	0.300 ± 0.004	1.10 ± 0.02	0.180 ± 0.001		
100	27.00 ± 0.05	0.37 ± 0.01	6.50 ± 0.05	0.270 ± 0.005	1.50 ± 0.05	0.320 ± 0.005

dx.doi.org/10.1021/jp506194y | J. Phys. Chem. C 2014, 118, 19484–19491

Table 3. Summary of Decay Parameters Best Fitted to the Total Decay Rate, Equation 6, for the Uncoupled and the Coupled Samples

τ	τ_{NR0} (ns)	τ_{Rt} (μs)	τ_{Rs} (μs)	$m - n$	m	ΔE (meV)
τ_{Vp}	27.6 ± 3.0	4.3 ± 1.0	0.065 ± 0.002	0.75 ± 0.11	2.99 ± 0.15	19.95 ± 2.9
τ_{im}	0.010 ± 0.001	23.4 ± 1.2	0.039 ± 0.005	1.40 ± 0.03	17.54 ± 1.5	37.24 ± 0.8
τ_1	0.042 ± 0.03	87.15 ± 1.2	0.0216 ± 0.003	2.07 ± 0.02	12.88 ± 0.8	55.06 ± 0.53

$$\frac{1}{\tau(T)} = \frac{1}{\tau_R(T)} + \frac{1}{\tau_{NR}(T)} \tag{6}$$

where $\tau(T)$ is the total exciton relaxation time and

$$\tau_R(T) = \tau_{Rt}\left[\frac{1 + (g_s/g_t)e^{-\Delta E/k_BT}}{1 + (g_s/g_t)(\tau_{Rt}/\tau_{Rs})e^{-\Delta E/k_BT}}\right] \tag{7a}$$

$$\tau_{NR}(T) = \tau_{NRt}(T)\left[\frac{1 + (g_s/g_t)e^{-\Delta E/k_BT}}{1 + (g_s/g_t)(\tau_{NRt}(T)/\tau_{NRs}(T))e^{-\Delta E/k_BT}}\right] \tag{7b}$$

with

$$\Delta E = (m - n)E_p \tag{7c}$$

$$\tau_{NRs}(T) = \tau_{NR0}[\exp(E_p/k_BT) - 1]^n$$
$$\tau_{NRt}(T) = \tau_{NR0}[\exp(E_p/k_BT) - 1]^m \tag{7d}$$

τ_{Rs} and τ_{Rt} are radiative lifetimes, and τ_{NRs} and τ_{NRt} are nonradiative lifetimes of exciton decays from singlet and triplet states, respectively, into the ground state or a trap state; g_s/g_t is the degeneracy ratio (equal to 1/3 in the singlet−triplet case); m denotes number of phonons emitted from the triplet state, and n the number of phonons emitted from the singlet state for the exciton to complete the nonradiative transition and decay to the ground state; ΔE is the lowest 1S−1S exciton splitting energy; E_p is the LO-phonon energy which in PbS is equal to 26.6 meV;[17] and τ_{NR0} is a time constant for the thermal (nonradiative) decay of excitonic electrons into a trap or surface state via the emission of n or m phonons ($m > n$).

Peak 1 in Figure 3 is characterized by three parameters: the distribution function $\Psi_{I1}(T)$, the center (most probable) lifetime τ_1, and the line width $\Delta\tau_1$ or the fwhm, where fwhm $\approx 1.665\Delta\tau_1$. The Arrhenius plot of the best fit to eq 6 of τ_1, peak 1, is shown in Figure 4 and the obtained parameters are listed in Table 3. That table also shows the values of the same parameters calculated from the Q-channel mean lifetimes (τ_{im}) best-fitted to the discrete variational model used to seed the spectrum of Figure 3. For reference, it also shows those parameter values calculated from the Voigt broadening lifetimes (τ_{Vp}) of the uncoupled sample. The lowest 1S−1S exciton splitting energy was found to be 55 meV which is larger than those found by other groups (~30 meV[8,9]) that neglected nonradiative lifetimes, thereby possibly measuring lower effective radiative deexcitation activation energies/barrier heights (eqs 6 and 7) and rendering the transition picture between the singlet and triplet states through intermediate interactions with adjacent trap states hard to quantify. The large coupled sample ratio τ_{Rt}/τ_{Rs} = 87.15/0.0216 (Table 3) physically indicates that the nonradiative recombination rate

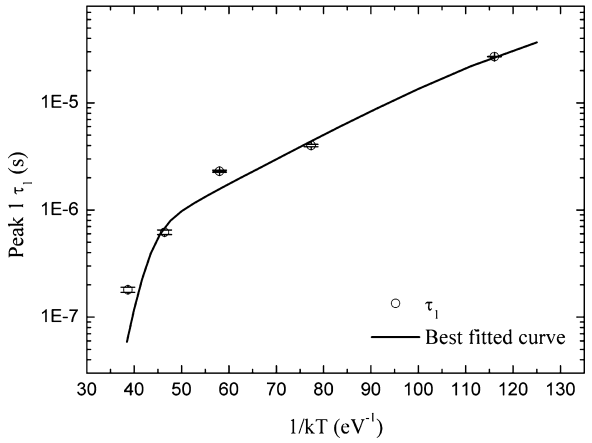

Figure 4. Arrhenius plot of peak 1 total exciton lifetime τ_1 best-fitted with eq 6.

is much lower than in the case of quasi-isolated excitons in the uncoupled sample where τ_{Rt}/τ_{Rs} = 4.3/0.065.

As in the case of uncoupled PbS CQDs, peak lifetime values of the coupled QD system can be used to probe the exciton energy manifold and the associated radiative and nonradiative decay pathways. The temperature-dependent fwhm is sensitive to exciton interactions leading to energy loss mechanisms. Specifically, in PbS CQDs with a short interdot distance ("coupled"), the peak 1 fwhm is associated with exciton−phonon scattering leading to exciton delocalization and trapping in QD surface states. In the statistical thermalization limit, the probability of exciton trapping, $P_t(T)$, can be expressed as a result of a trapping rate equation analogous to electronic carrier trapping in a conventional semiconductor[18]

$$P_t(T) = \frac{N_t(T)}{N_0} = 1 - e^{-E_T/kT} \tag{8}$$

where N_0 is the total number density of sites or states that can act as exciton traps and $N_t(T) = N_0(1 - e^{-E_T/kT})$ is the number density of occupied exciton traps. E_T is the trap thermal ionization energy for excitons. At very low temperatures all traps are filled and $P_t \approx 1$. As the temperature increases, the probability of exciton trapping decreases and the occupied trap density also decreases as more excitons are thermally ionized. This process is mediated through phonon interactions assisting in exciton detrapping. As a consequence, this mechanism contributes to exciton decay and lifetime thermalization broadening. It predicts the following fwhm temperature dependence:

$$\text{fwhm}(T) = \Delta\tau_0[1 - \exp(-E_T/kT)] + \Delta\tau_I \tag{9}$$

Figure 5 shows excellent best-fit results of eq 9 to the fwhm of peak 1 in Figure 3. The fwhm increases with decreasing temperature, which is consistent with the increasing exciton trapping probability or, rather, the decreasing exciton detrapping probability due to decreasing phonon populations

dx.doi.org/10.1021/jp506194y | J. Phys. Chem. C 2014, 118, 19484−19491

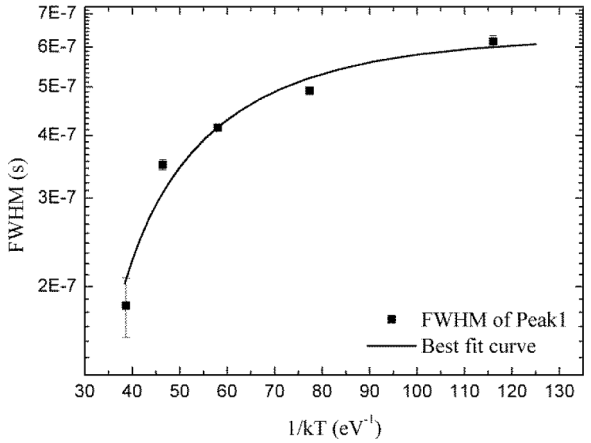

Figure 5. Arrhenius plot of the peak 1 fwhm(T) in Figure 1 best fitted to eq 9. The fitting parameters are E_T = 35.34 meV, $\Delta\tau_0$ =1.66 μs, and $\Delta\tau_I$ = −1.027 μs.

and exciton−phonon interactions. The trap thermal ionization energy E_T was found to be 35.34 meV. $\Delta\tau_0$ is a measure of lifetime broadening due to the exciton residence time in the limit of no exciton−phonon interactions, a function of trap density, and was best fitted to be 1.66 μs, while $\Delta\tau_I$ = −1.027 μs is probably associated with PbS QD size distribution effects.[9,11]

Peak 2: Exciton Tunneling and Migration. The appearance of the shorter-lifetime distribution at $T \leq 200$ K is qualitatively consistent with excitonic hopping from smaller to larger colloidal PbS QDs where excitons relax at faster rates than those in the original QD, also consistent with the size-dependent radiative decay in PbS CQDs.[19,20] Figure 3 shows that peak 2, like peak 1, shifts to longer-lifetime values with decreasing temperature following its emergence at or around T = 200 K. The probability rate P_{ij} (s^{-1}) for exciton-to-exciton hopping, resulting in transitions from a smaller-QD higher exciton energy state (i) to a larger nearest-neighbor-QD unoccupied lower-energy state (j) is

$$P_{ij} = \frac{1}{\tau_{ij}} = \nu \exp(-\gamma_{ij} R_{ij}) \tag{10}$$

where ν is the attempt frequency, R_{ij} is the distance between QDs i and j, and γ_{ij} is related to the energy barrier which separates the QDs at sites I -and j.[21] Given that the PbS inter-QD space is filled with a nonconducting colloid, hopping can be identified with tunneling from one excitonic wave function to that of a neighboring exciton, in which case R_{ij} can be thought of as the barrier thickness and the tunneling probability rate can be written in the WKB approximation as[22]

$$P_{ij} = \nu \exp[-2R_{ij}\sqrt{(2m^*/\hbar^2)(V - E_i)}\,] \tag{11}$$

where m^* is the effective mass in the barrier layer, V is the energy barrier height, and E_i is the quantum energy level of the tunneling exciton. In a thermodynamic bath of temperature T, one may expect the amount of energy required for barrier height climbing and inter-QD tunneling to be supplied by a characteristic thermal energy of the ambient (colloidal) medium

$$q(V - E_i) = k_B T_0 \tag{12}$$

Therefore, eq 11 can be written in terms of the tunneling time

$$\tau_{ij} = \frac{1}{P_{ij}} = \nu^{-1} \exp[2R_{ij}\sqrt{(2m^* k_B/q\hbar^2)T_0}\,] \tag{13}$$

However, this expression would hold only for transition events without constraints among adjacent excitons which would exhibit a single tunneling time τ_{ij}. The fact that hopping kinetics has been associated with stretched exponential behavior of the Kohlrausch type[23] in quantum dot photoluminescence intensity[21,24]

$$I(t) = I_0 \exp[-(t/\tau)^{\beta}] \tag{14}$$

is an indicator of a strongly correlated exciton system with hierarchical constraints, such that faster degrees of freedom (here, tunneling rates) successively constrain slower ones, possibly as excited energy states of nearest-neighbor excitons become occupied and the effective tunneling distance/barrier R_{ij} increases. This physical situation has been shown to involve ergodic relaxation times which increase as the temperature decreases in glassy systems,[25] a trend which is also evident with peak 2 in PbS CQDs. Palmer et al. have shown that in hierarchical dynamics systems satisfying the foregoing conditions, a relaxation time behavior of type $\tau \approx \exp[A/(T - T_0)]$ holds around a characteristic (glass) transition temperature (a Vogel−Fulcher-type law[26,27]). In view of the structure of eq 13 an analogous treatment of the tunneling configuration which satisfies eq 14 and the ergodic relaxation time increase with decreasing temperature leads to a modified eq 13:

$$\tau_{ij}(T) = \frac{1}{P_{ij}} = \nu^{-1} \exp[2R_{ij}\sqrt{A(2m^* k_B/q\hbar^2)T_0/(T - T_0)}\,] \tag{15}$$

The probability rate for exciton-to-exciton hopping in eqs 10−15 is related to the confinement energy (∼0.1 eV) and the activation energies (<50 meV).[4] Therefore, eq 15 can be simplified for temperatures $T \gg T_0$ such as those used in our experiments as

$$\tau_{ij}(T) = \frac{1}{P_{ij}} = \nu^{-1} \exp[2R_{ij}\sqrt{A_{ij}(2m^* k_B/q\hbar^2)T_0/T}\,] \tag{16}$$

A_{ij} is associated with the number of excitons at level E_i which attain a particular state E_j following a tunneling event. This equation is of the form

$$\tau_2(T) = \tau_0 \exp\left[\left(\frac{CT_0}{T}\right)^p\right] \tag{17}$$

with p = 0.5. This theoretical prediction is in excellent agreement with the experimental result p = 0.48 derived from peak 2 as shown in Figure 6. This result is also consistent with Romero and Drndic,[6] who reported the temperature-dependent hopping conductivity domination of exciton transport in PbSe QDs where a thermally activated process controls charge transport when T > 265 K. When T < 200 K, conduction was found to be due to Efros-Shklovskii VRH with a typical $T^{-1/2}$ dependence of the conductivity, increasing the charge carrier probability for hopping across distant dots.[28] As T decreases below 200 K, the transport of excitons from a smaller QD at a higher-energy state to a lower-energy state of nearby larger QDs was found to become more efficient.

Peak 3 emerges in Figure 3 at 100 K, which represents the limit of our experimental cryogenic capabilities. However, lower

dx.doi.org/10.1021/jp506194y | J. Phys. Chem. C 2014, 118, 19484−19491

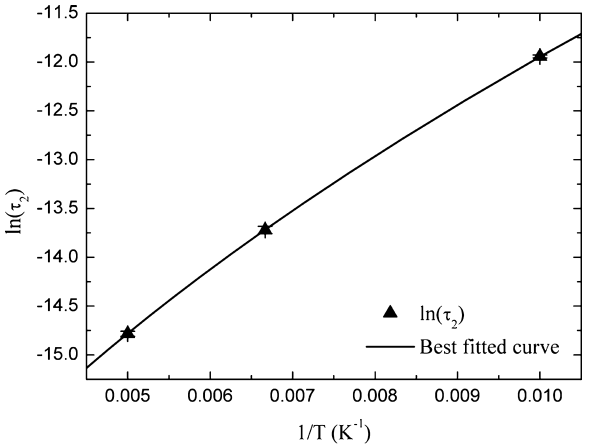

Figure 6. Arrhenius plot of $\ln(\tau_2)$ (peak 2 in Figure 1), best fit to eq 17. Slope p = 0.48.

temperatures are needed to probe the physical processes associated with this peak.

CONCLUSIONS

A generalized variational inverse method capable of resolving simultaneous multipath deexcitation mechanisms of coupled (interacting) PbS CQD samples was developed and applied to the reconstruction of continuous excitonic lifetime Voigt spectra using the phase of frequency-scanned laser photocarrier radiometry. From two reconstructed lifetime peak sequences in the temperature range of 300 K $\geq T \geq$ 100 K, it was found that overall radiative deexcitation is greatly enhanced at low temperatures. However, at T = 100 K only 5.5% of all excitons decay radiatively through the mechanism dominating room-temperature decay. The fraction of exciton population decaying through the available pathways at room temperature rapidly decreases at lower temperatures as the result of overall radiative enhancement, and reaches only 1.14% at T = 100 K. The analysis of Voigt lifetime distribution peak 1 and its associated fwhm over the full 300−100 K range was consistent with exciton−phonon-mediated radiative and nonradiative decay channels, whereas lower-temperature Voigt lifetime peak 2 and its fwhm identified exciton tunneling and migration from small QDs at a higher energy state to lower energy states of nearby larger QDs as the dominant deexcitation mechanism. The two simultaneous peak sequences further yielded much lower nonradiative recombination rates for coupled PbS CQDs than for uncoupled samples, thereby making the PCR-phase lifetime reconstruction method a probe and control which can be used to optimize lead salt CQD solar-cell fabrication design through improved understanding and chemical-fabrication-controlled minimization of nonradiative carrier losses which currently limit photovoltaic efficiency.

AUTHOR INFORMATION

Corresponding Author

*Phone: 001-(416)-978-1287. Fax: 001-(416)-266-7867. E-mail: mandelis@mie.utoronto.ca.

Notes

The authors declare no competing financial interest.

ACKNOWLEDGMENTS

A.M. is grateful to the Natural Sciences and Engineering Research Council (NSERC) for a Discovery grant, to the Canada Foundation for Innovation (CFI) for equipment grants, to the Canada Research Chairs Program, and to the 1000 Talents Program of the Government of China. J.W. is grateful to the China Scholarship Council (CSC) for an international student grant, the National Natural Science Foundation of China (grant no. 61379013), and the Central-University Basic Research Funds of UESTC (grant no. ZYGX2012Z006). Sjoerd Hoogland and Edward H. Sargent are acknowledged for CQD sample contributions and valuable discussions.

REFERENCES

(1) Tang, J.; Sargent, E. H. Infrared Quantum Dot for Photovoltaics: Fundamentals and Recent Progress. *Adv. Mater.* **2011**, *23*, 12−29.

(2) Pattantyus-Abraham, A. G.; Kramer, I. J.; Barkhouse, A. R.; Wang, X.; Konstantatos, G.; Debnath, R.; Levina, L.; Raabe, I.; Nazeeruddin, M. K.; Grätzel, M.; Sargent, E. H. Depleted-Heterojunction Colloidal Quantum Dot Solar Cells. *ACS Nano* **2010**, *4*, 3374−3380.

(3) Leschkies, K. S.; Beatty, T. J.; Kang, M. S.; Norris, D. J.; Aydil, E. S. Solar Cells Based on Junctions Between Colloidal PbSe Nanocrystals and Thin ZnO Films. *ACS Nano* **2009**, *3*, 3638−3648.

(4) Guyot-Sionnest, P. Electrical Transport in Colloidal Quantum Dot Films. *J. Phys. Chem. Lett.* **2012**, *3*, 1169−1175.

(5) Clark, S. W.; Harbold, J. M.; Wise, F. W. Resonant Energy Transfer in PbS Quantum Dots. *J. Phys. Chem. C* **2007**, *111*, 7302−7305.

(6) Romero, H. E.; Drndic, M. Coulomb Blockade and Hopping Conduction in PbSe Quantum Dots. *Phys. Rev. Lett.* **2005**, *95*, 156801.

(7) Andreakou, P.; Brossard, M.; Li, C.; Bernechea, M.; Konstantatos, G.; Lagoudakis, P. G. Size- and Temperature-Dependent Carrier Dynamics in Oleic Acid Capped PbS Quantum Dots. *J. Phys. Chem. C* **2013**, *117*, 1887−1892.

(8) Espiau de Lamaestre, R.; Bernas, H.; Pacifici, D.; Franzo, G.; Priolo, F. Evidence for a"Dark Exciton"State of PbS Nanocrystals in a Silicate Glass. *Appl. Phys. Lett.* **2006**, *88*, 181115.

(9) Gaponenko, M. S.; Lutich, A. A.; Tolstik, N. A.; Onushchenko, A. A.; Malyarevich, A. M.; Petrov, E. P.; Yumashev, K. V. Temperature-dependent Photoluminescence of PbS Quantum Dots in Glass: Evidence of Exciton State Splitting and Carrier Trapping. *Phys. Rev. B* **2010**, *82*, 125320.

(10) Wehrenberg, B. L.; Wang, C.; Guyot-Sionnest, P. Interband and Intraband Optical Studies of PbSe Colloidal Quantum Dots. *J. Phys. Chem. B* **2002**, *106*, 10634−10640.

(11) Wang, J.; Mandelis, A.; Melnikov, A.; Hoogland, S.; Sargent, E. H. Exciton Lifetime Broadening and Distribution Profiles of PbS Colloidal Quantum Dot Thin Films Using Frequency- and Temperature-Scanned Photocarrier Radiometry. *J. Phys. Chem. C* **2013**, *117*, 23333−23348.

(12) Mandelis, A.; Batista, J.; Shaughnessy, D. Infrared Photocarrier Radiometry of Semiconductors: Physical principles, Quantitative Depth Profilometry, and Scanning Imaging of Deep Subsurface Electronic Defects. *Phys. Rev. B* **2003**, *67*, 205208.

(13) Zhitomirsky, D.; Kramer, I. J.; Labelle, A. J.; Fischer, A.; Debnath, R.; Pan, J.; Bakr, O. M.; Sargent, E. H. Colloidal Quantum Dot Photovoltaics: The Effect of Polydispersity. *Nano Lett.* **2012**, *12*, 1007−1012.

(14) Pattantyus-Abraham, A. G.; Kramer, I. J.; Barkhouse, A. R.; Wang, X.; Konstantatos, G.; Debnath, R.; Levina, L.; Raabe, I.; Nazeeruddin, M. K.; Grätzel, M.; Sargent, E. H. Depleted-Heterojunction Colloidal Quantum Dot Solar Cells. *ACS Nano* **2010**, *4*, 3374−3380.

(15) Xia, J.; Mandelis, A. Direct-search Deep Level Photothermal Spectroscopy: An Enhanced Reliability Method for Overlapped Semiconductor Defect State Characterization. *Appl. Phys. Lett.* **2010**, *96*, 262112.

(16) Xia, J.; Mandelis, A. Broadening Effects and Ergodicity in Deep Level Photothermal Spectroscopy of Defect States in Semi-insulating GaAs: A Combined Temperature-, Pulse-rate-, and Time-domain Study of Defect State Kinetics. *J. Appl. Phys.* **2009**, *105*, 103712.

(17) Kraus, T. D.; Wise, F. W. Coherent Acoustic Phonons in a Semiconductor Quantum Dot. *Phys. Rev. Lett.* **1997**, *79*, 5102−5105.
(18) Mandelis, A.; Xia, J. Deep Level Photothermal Spectroscopy: Physical Principles and Applications to Semi-insulating GaAs Band-gap Multiple Trap States. *J. Appl. Phys.* **2008**, *103*, 043704.
(19) Chen, Y.; Yu, D.; Li, B.; Chen, X.; Dong, Y.; Zhang, M. Size-dependent Radiative Emission of PbS Quantum dots Embedded in Nafion Membrane. *Appl. Phys. B* **2009**, *95*, 173−177.
(20) Litvin, A. P.; Parfenov, P. S.; Ushakova, E. V.; Fedorov, A. V.Size-Dependent Room-Temperature Luminescence Decay from PbS Quantum Dots. *Proceedings of SPIE 8564, Nanophotonics and Micro/Nano Optics*, 2012, 85641Z.
(21) Roman, H. E.; Pavesi, L. Monte Carlo Simulations of the Recombination Dynamics in Porous Silicon. *J. Phys.: Condens. Matter* **1996**, *8*, 5161−5187.
(22) Tackeuchi, A.; Kuroda, T.; Mase, K.; Nakata, Y.; Yokoyama, N. Dynamics of Carrier Tunneling Between Vertically Aligned Double Quantum Dots. *Phys. Rev. B* **2000**, *62*, 1568.
(23) Kohlrausch, R. Nachtrag ueber die elastische Nachwirkung beim Cocon und Glasfaden. *Ann. Phys. (Leipzig)* **1847**, *12*, 393−399.
(24) Lifshitz, E.; Sirota, M.; Porteanu, H. Continuous and Time-resolved Photoluminescence Study of Lead Sulfide Nanocrystals, Embedded in Polymer Film. *J. Cryst. Growth* **1999**, *196*, 126−134.
(25) Palmer, R. G.; Stein, D. L.; Abrahams, E.; Anderson, P. W. Models of Hierarchically Constrained Dynamics for Glassy Relaxation. *Phys. Rev. Lett.* **1984**, *53*, 958−961.
(26) Vogel, H. Das Temperature-abh ngigketsgesetz der viskosit t von flüssigkeiten. *Phys. Z.* **1921**, *22*, 645.
(27) Fulcher, G. S. Analysis of Recent Measurements of the Viscosity of Glasses. *J. Am. Ceram. Soc.* **1925**, *8*, 339.
(28) Shklovskii, B. I.; Efros, A. L. *Electronic Properties of Doped Semiconductors*; Springer-Verlag: Berlin, 1984.